Multiscale description and prediction of the thermomechanical behavior of multilayered plasticized PVC under a wide range of strain rate

Christelle Bernard, Nadia Bahlouli, Christiane Wagner-Kocher, Jian Lin, Saïd Ahzi, Yves Rémond

Multiscale description and prediction of the thermomechanical behavior of multilayered plasticized PVC under a wide range of strain rate

C.A. Bernard[a,b], N. Bahlouli[b], C. Wagner-Kocher[c,d*], J. Lin[b], S. Ahzi[b], Y. Rémond[b]

[a] FRIS, Tohoku University, Sendai, Japan

[b] ICube, Université de Strasbourg/CNRS, 2 rue Boussingault, 67000 Strasbourg, France.

[c] Université de Strasbourg - UHA Mulhouse, LPMT, 11 rue Alfred Werner, 68093 Mulhouse Cedex, France.

[d] LMGC, Univ. de Montpellier, CNRS, Montpellier, France.

[*]Corresponding author : Christiane Wagner-Kocher

LMGC – Laboratoire de Mécanique et génie Civil / CNRS

Université de Montpellier

860 rue Saint Priest,

34095 Montpellier, France

christiane.wagner-kocher@umontpellier.fr

Abstract

Plasticization of polymers largely contributed to their worldwide utilization, especially for automotive crashworthiness, by making them a more ductile material. For such applications, a clear understanding of the mechanical properties evolution over a large range of strain rate and temperature is needed. In this study, we investigate a plasticized poly(vinyl chloride) (PPVC) manufactured through a multi-layered process for the automotive industry. Analysis of the microstructure before and after mechanical testing, at different temperature and strain rate, highlighted on the presence of sodium aluminosilicate within material microstructure. After thermal degradation analysis, these particles seem to be the only one to remain at high temperature. Moreover, it is important to mention that for the possible applications of this material, the temperature range is around the glass transition region leading. Thus, careful attention should be focused on the evolution of the material properties and on the way to model them. Numerical prediction of the storage modulus and yield stress using homemade models show a good agreement with the experimental data. More, these models will make reliable the use of these materials over a wide range of temperatures and strain rates that are difficult to obtain by experience, such as intermediate strain rates between quasi static and dynamic loading.

Keywords

Plasticized PVC; Multiscale, Strain rate; Temperature

1. Introduction

Since the early 1970s, the part polymeric materials play in the automotive industry has strongly increased to reduce the mass of vehicles. Thus, the fuel consumption is lowered and performances are improved in terms of noise, shock absorption or lifetime. Among the polymers used in the automotive industry, poly(vinyl chloride) (PVC) is widely used for crashworthiness applications. At room temperature, PVC is a glassy polymer. Several works [1–3] measured the glass transition of PVC around 82°C. However, Pezzin et al. [4] showed that the glass transition of PVC is dependent on its molecular weight. This can be explained by the PVC chain stiffness and the free volume theory [5,6]. The conditions of polymerization are such that all samples have the same degree of syndiotacticity. Pezzin et al. [4] found that the glass transition temperature increases rapidly and asymptotically reaches the limiting value $\mathrm{T_g^{\infty}} = 78\ ^{\circ}\mathrm{C}$.

The PVC used in the automotive industry is generally modified by plasticizing to obtain flexible PVC. This is the so-called plasticized PVC (PPVC), where the effects of weather, road and driving conditions are minimized. In PPVC, powdered resin is mixed with each of a stabilizer, plasticizer, lubricant and dioctyl phthalate that explain the thermal stability of PPVC at processing temperatures [7, 8,9].

Investigations of the mechanical response, plasticizer effect and morphology of PPVC have been of particular interest to academic researchers and industrialists because of the widespread use of PPVC in automotive crashworthiness. Many authors [10, 11, 12, 22] investigated the strain rate dependence of PVC and PPVC with a high-level of plasticizer, from quasi-static to dynamic loading at room temperature. They also investigated the temperature sensitivity of both materials for a strain rate of $10^{-2}\ s^{-1}$. For all strain rates tested, at room temperature PVC exhibits a glassy polymer behavior, whereas PPVC shows a change of behavior between the quasi-static and dynamic loading. Thus, at low strain rates, PPVC reveals a rubbery polymer behavior and at high strain rates, the mechanical response of PPVC is glassier. However, at room temperature strain softening of PPVC is not observed, unlike PVC. Investigation of the temperature sensitivity clearly shows a change in the mechanical response of PPVC. For temperatures lower than -40°C, PPVC exhibits a glassy polymer response. The yield stress is clearly identified and is followed by strain softening. Between -20°C and 0°C, the

mechanical response of PPVC is less glassy and a rubbery mechanical behavior is identified for temperatures above 21°C. These authors also showed that the yield stress is bi-linearly dependent on the log of the strain rate. Wang et al. [1] investigated the strain rate dependence of PPVC. Loading-unloading compressive tests at constant strain rates highlight a viscoelastic behavior of PPVC. Mulliken et al. [13] performed dynamic mechanical analyses and quasi-static and dynamic uniaxial compressive tests on PVC and 20 % PPVC. They found that the addition of 20 % of plasticizers into the PVC blend decreased the glass transition temperature to 22°C. Moreover, for this level of plasticizer at room temperature, the PPVC exhibits a glassy behavior at high strain rates and the yield point is followed by strain softening. This is in contrast to the PPVC investigated by Kendall and Siviour [10, 11]. Thus, the percentage of plasticizer in the PPVC blend is of great importance for its mechanical properties. The effects of the plasticizer content on the material properties of PPVC have been investigated previously [14,15] and several observations have been made. In addition to the previous observations, the addition of a plasticizer to the PPVC blend decreases the glass transition temperature [3,16,17]. Moreover, while the addition of a plasticizer improves the elongation at break and increases both the fracture energy and the Poisson's ratio, it decreases the elastic modulus, the yield stress and the hardness of the material [7,8,18-20]. Thus, the mechanical behavior of PPVC exhibits a triple dependence on strain rate, temperature and plasticizer level. Thus, a literature review highlights strong differences depending on the PPVC and its plasticizer content. Varughese et al. [7] and Thomas et al. [21] investigated the tensile and tear fracture surfaces. Scanning electron microscopy observation on fractured surface after tensile tests showed ductile-type failure, mainly due to shear fracture with high plastic deformation, whereas the tear fractography brings out the presence of sine waves.

The purpose of this paper is to characterize and analyze the thermomechanical behavior and the deformation mechanisms of PPVC sheets obtained by a layered process. This process is not useful for the dynamic loading. Because the manufacturing process strongly influences the mechanical properties of a material, it is necessary to analyze the strain rate and temperature sensitivity of a layered PPVC at different scales. The studied PPVC is destined to components designed for the automotive industry. Thus, the PPVC structure will be submitted to high strain rates. The thermomechanical behavior of the material and its morphology were characterized: detailed thermal and mechanical analyses being performed over a wide range

of strain rates and temperatures to . To improve the use of the layered PPVC, we propose a predictive modeling of the modulus and the threshold stress.

2. Materials and methods

2.1. Materials

The PPVC studied in this paper is composed of 50 % PVC, 40 % plasticizer and 10 % additives. The material was manufactured by Faurecia using an innovative layered process and provided as PPVC sheets of 1 mm thickness.

2.2. Morphology

Micrographs were taken before and after mechanical characterization, to observe modifications of the morphological aspects and defects of PPVC along its thickness. Chemical microanalyses of energy dispersive X-ray spectra (EDS) were registered and microstructure analysis was carried out using Energy Dispersive X-ray Microanalysis together with Scanning Electron Microscopy (SEM; JEOL 6700F). Sections were cut from the gauge length before and after tensile tests. The fractured surfaces were obtained by breaking PPVC specimens in liquid nitrogen to minimize the development of plastic deformation. The topology of the fracture surfaces was directly observed after iridium coating. The presence and the sizes of voids were analyzed using ImageJ and compared, before and after tensile tests for three specimens.

2.3. Thermal analysis

The thermal stability of PPVC was evaluated by thermogravimetric analysis (TGA) on a METTLER TOLEDO TGA/DSC1 machine, with the STAR system, operated in air from 40°C to 1000°C at a heating rate of 20°C/min. The mass of the specimens ranged between 15 and 25 mg. The mass loss and temperature during the test were recorded. The accuracy of the weighing machine is 1 µg.

Differential Scanning Calorimetry (DSC) tests were conducted on a METTLER TOLEDO DSC1 machine with the STAR System and a HSS8 sensor. These tests characterize the transition temperatures and analyze the phase miscibility of the material. The mass of the tested specimens was approximately 15 mg. The heating cycle was carried out for a temperature

range from -150°C to 250°C with a heating rate of 10°C/min. A second scan was performed at the end of the first scan after quenching, to evaluate the polymer properties after removing the sample thermal history. This is erased when the material is heated above its glass transition temperature.

Dynamic mechanical analyses (DMA) were conducted under tensile loading at 1 Hz for a temperature range from -100°C to 120°C. The glass transition temperature range was first determined by testing the sample using a 2°C/min dynamic temperature sweep at 0.2% strain and 1 Hz [23, 24]. The evolution of the storage modulus, loss modulus and tan δ (the ratio between the loss and storage moduli) were investigated over the range of temperature studied. The glass transition temperature measured by DSC and DMA were compared using different analysis methods to better understand the discrepancies that exist between these two thermal techniques.

2.4. Mechanical characterization

Quasi-static uniaxial tensile tests

For the quasi-static strain rate tests, uniaxial quasi-static tensile tests were conducted using an INSTRON 3384 universal testing machine equipped with a temperature chamber (500 Series Chambers) to perform mechanical tests at different temperatures. Tests were carried out at constant displacement rates, at 50 and 500 mm/min for different constant temperatures (-30°C, 0°C, 23°C, 85°C). The stress-strain behavior of the samples was determined from the load-displacement data of the tensile device. At the yield point, identified on the stress-strain curves as the intersection point between the viscoelastic behavior slope and the viscoplastic behavior slope, these displacement rates lead to true strain rates of 0.03 s^{-1} and 0.3 s^{-1} respectively. The test specimens are cut from PPVC sheets by Faurecia. The specimen geometry follows the standard ASTM D412 classically used in international industries. For both temperature and strain rate, at least five samples were tested.

Dynamic uniaxial compressive tests

For the high strain rates, uniaxial compression tests were carried out on a homemade Split Hopkinson Pressure Bar (SHPB) [25, 27] at three temperatures (-30°C, 23°C, 85°C) and two ranges of strain rates. Two devices, one for low and one for high temperatures, were adapted

on our SHPB. At high temperatures, the sides of the two bars in contact with the specimen were positioned in a homemade furnace containing two electrical resistances. For low temperatures, the specimen was sandwiched between the two bars inside a home-made temperature chamber. Then, the specimen and a short part of the bars were cooled to below -30°C by the addition of liquid nitrogen to the chamber. The addition of technical alcohol helps to maintain the thermal equilibrium during the tests. Four thermocouples inserted in the temperature chamber allow the temperature inside the oven to be controlled. To reach a thermal equilibrium, the samples were heated or cooled in the appropriate chamber and maintained at the target temperature for 15 min before testing [25, 30].

The test fixture is composed of three 22 mm diameter steel bars. The input and output bars are 3 m long and the strikers are 0.5 m and 1 m long, to reach a wider range of strain rates. These strikers are launched with an air gun against the incident bar to generate the incident pressure pulse. On impacting the input bar, the striker generates an incident pulse $\varepsilon_i(t)$. Once this pulse reaches the specimen, one part $\varepsilon_r(t)$ is reflected into the incident bar, the other part $\varepsilon_t(t)$ goes through the specimen and is transmitted to the output bar. According to the wave propagation theory, the stress and particle velocity can each be calculated at every section of the bars. In particular, they are shifted from the gauge location to both bar/specimen interfaces considering two superposed waves propagating in opposite directions at a velocity C_b, which is the speed of sound into the bars when dispersion is neglected. This velocity was measured during a conventional SHPB test without specimen [28, 29]. Thus, assuming that the bars are linear with a constant section and that the deformation and forces are homogenous within the sample, we can apply the classical elastic wave propagation theory. The nominal strain rate $\dot{\varepsilon}_n$, strain ε_n and stress σ_n are given by:

$$\dot{\varepsilon}_n(t) = -\frac{2C_b}{L_s(0)}\varepsilon_r(t) \tag{1}$$

$$\varepsilon_n(t) = -\frac{2C_b}{L_s(0)}\int_0^t \varepsilon_r(\tau)\, d\tau \tag{2}$$

$$\sigma_n(t) = 2E_b\frac{A_b}{A_s}\left(\varepsilon_i(t) + \varepsilon_r(t) + \varepsilon_t(t)\right) \tag{3}$$

where E_b is the Young modulus of the bar, $L_s(0)$ is the initial length of the sample, A_b and A_s are the cross-sectional area of the bar and the sample, respectively. According to *v*, the

polymer viscosity, the true strain and true stress are identified from the nominal measurement:

$$\varepsilon_t(t) = -\ln\big(1+\varepsilon_n(t)\big) \tag{4}$$

$$\sigma_t(t) = \sigma_n(t)\big(1-\varepsilon_n(t)\big)^{2\nu} \tag{5}$$

Cylindrical specimens with a diameter of 10 mm, cut from the PPVC sheets, were tested to investigate their dynamic thermomechanical behavior. For each condition (temperature, strain rate), at least five samples were tested.

3. Results and Discussion

3.1. Microstructural characterization

The fracture surface morphology was observed by scanning electron microscopy at different visualization scales. Figure 1 shows SEM micrographs of the fractured surfaces taken perpendicular to the loading direction before (Figure 1a) and after (Figure 1b) quasi-static tensile tests. Due to the cooling of samples in liquid nitrogen before breakage, the material exhibits brittle fracture. The fractured surfaces reveal the presence of voids. Before testing, the percentage of voids within the specimen is around 4% and increased to 6.7% after testing. The number of small and middle size voids increase by 50% whereas the number of the larger voids is quite constant. However, it appears that their diameter highly increases (+150-200%) after testing.

For all the analyzed specimens, the voids are well distributed with the presence of the small and middle size voids mainly located at the bottom of the specimen and the larger size voids located in the specimen core. Because the voiding appears perfectly aligned along a line, their presence and position are probably related to degassing phenomena occurring at different time intervals of the manufacturing process of the PPVC sheets.

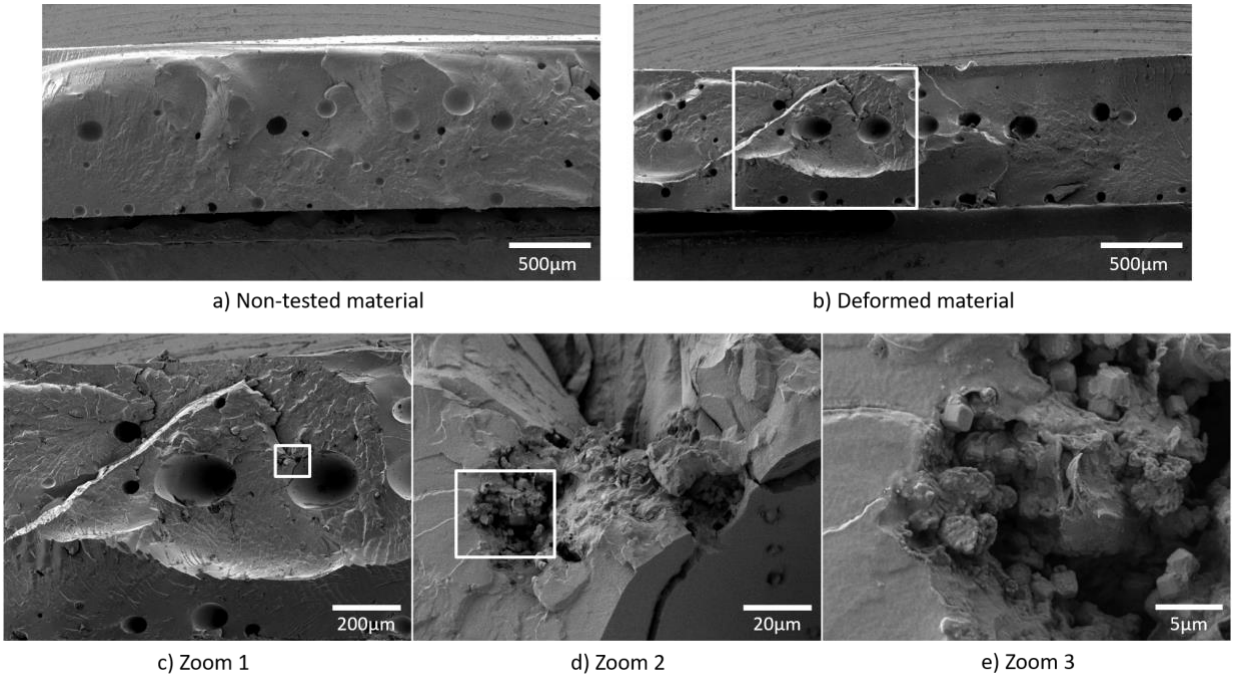

Figure 1: SEM micrographs of a) the fractured surface of virgin material, and b) after quasi-static tensile tests and c, d, e) gradual magnification of b) highlighting the presence of cubic clusters near the porosity.

Even though similar microstructures are observed before and after mechanical testing of the specimen, in terms of voids repartition, the fracture surface of the tested specimen (see Figure 1b) exhibits some irregularities unseen in the non-tested area (see Figure 1a). When we increase the magnification (see Figure 1c,d,e), voids with different shapes were observed. At higher magnification, clusters of cubic particles appear (see Figure 1e). The size of the cubic particle is approximately 1 μm^3.

Analysis by X-ray diffraction presented in Figure 2b will provide more information about sample constitution. The areas contained in the white squares shown in Figure 2a were analyzed. Sq1 corresponds to the fractured surface outside the cluster; Sq2 is taken from inside the cluster and S3 matches one cubic nodule. The results of X-ray patterns are presented in Figure 2b. SEM coupled with energy dispersive X-ray spectroscopy also allows highlighting of the chemical composition of the observed particles. Sq1 and Sq2 show similar chemical compositions while S3 demonstrates a higher oxygen peak and non-negligible representative peaks of Na, Al and Si. In the Sq2 zone, even if the presence of agglomerates is observed, the X-ray pattern shows very low contents of Na, Al and Si. These elements (O, Na, Al, Si) are proof of the presence of sodium aluminosilicate classically used as a stabilizing component of PVC melts [26].

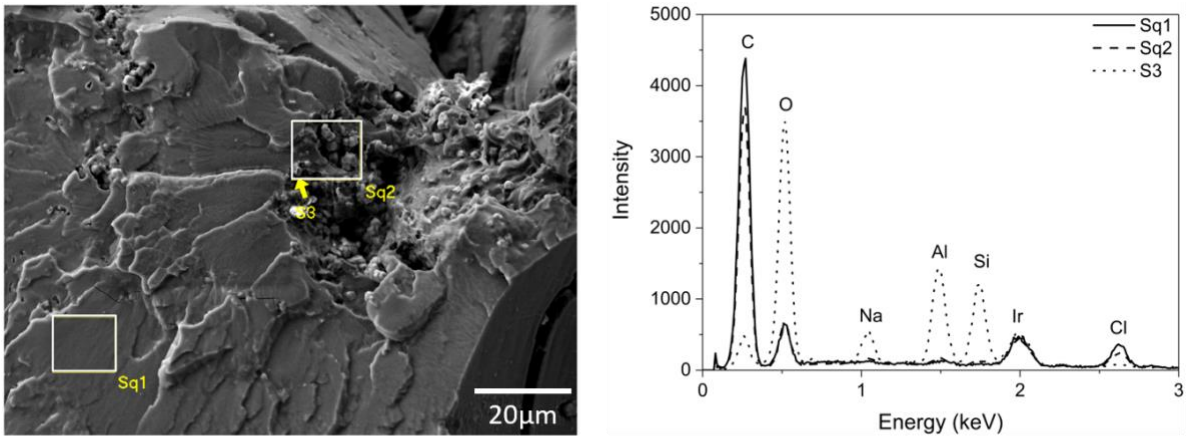

a) Presence of three microstructures into the specimen

b) X-ray pattern of the three microstructures

Figure 2: a) Identification of three microstructures in the PPVC studied and b) X-ray patterns of these three zones.

3.2. Thermogravimetric analysis

The thermal degradation of PPVC, characterized by TGA, is shown in Figure 3, for three specimens to evaluate the discrepancy seen in the material. The thermogravimetry (TG) curves show the percentage of mass loss versus temperature. The DTG curves are superposed onto the TG curves and indicate the rate of mass loss used to evaluate the degradation temperature of the material. Similarly to pure PVC [16, 32], the thermogravimetric curves of PPVC (see Figure 3a) show two degradation peaks around 330°C and 455°C. These correspond to a loss of 73.9%±2.1% and 15.4%±0.3% of the initial mass. This leads to a total mass loss of approximately 90 % for each tested specimen. The samples are thermally stable and the weight loss rate is almost equal to zero at temperatures below 250°C. Above this temperature, the decomposition rate falls and reaches a minimum of -13.97 (± 8%) $\%.min^{-1}$ at 329.8 (± 1.27%) °C. According to previous publications, [33-36], the first degradation step matches the dehydrochlorination of PVC, with the formation of hydrochloric acid (HCl) and conjugated polyene sequences of 5-25 double bonds. The second step is characterized by the formation of alkyne aromatic hydrocarbons and char residues, due to the rearrangement of polyene structures through cyclization and cross-linking reactions. When PPVC samples are heated above 500°C, their mass is stable. The residual weight fraction is 10.8%±2.1% and this can be related to the cubic particles observed during characterization of morphology.

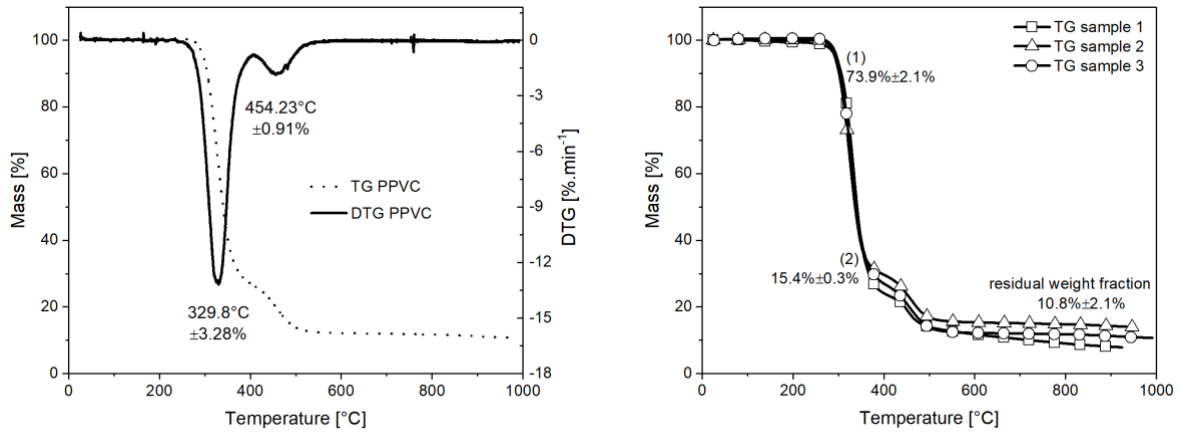

a) TG and DTG of PPVC sample

b) Superposition of three PPVC samples

Figure 3: Thermogravimetric curves of the PPVC sheets for each thickness.

The thermogravimetric curves obtained for each sample are plotted in Figure 3b. The two degradation steps are clearly identified. Between the three specimens studied, some discrepancies appear at the beginning of the second stage due to a difference of mass loss at the end of the first stage. This difference can be attributed to a variation in the quantity of HCl during the first step. Despite the difference of mass loss between the two degradation stages, the total degradation of the material is approximately the same at the end of the thermogravimetry analysis. According to the literature, the presence of plasticizers and additives in the PVC does not delay the first stage of deformation, however, it delays the second stage of the material degradation (from 454°C to 466°C for [16] and from 465°C to 515°C for [32]).

3.3. Differential Scanning Calorimetry (DSC)

Figure 4 shows the DSC thermograms of PPVC from -150°C to +250°C for three specimens, to evaluate the discrepancy in material properties induced by the layered process. The first heating run was carried out to remove the thermal history of the samples. The second heating run leads to the determination of the different thermal transitions of the studied polymer. The glass transition temperature of PPVC is characterized by an endothermic deviation from the baseline in the DSC thermogram. From the DSC tests, we assume that the glass transition temperature is given the midpoint of the heat-capacity shift. In the first scan, an endothermic deviation appears at approximatively -41°C. In the second scan, the first deviation, which corresponds to the glass transition temperature, is close to -32°C.

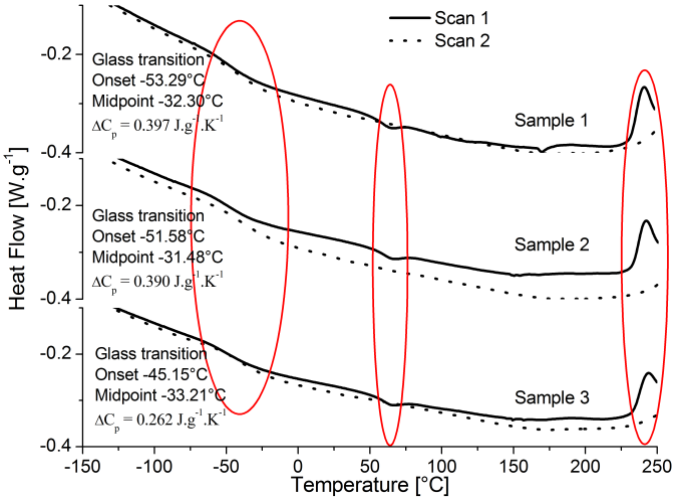

Figure 4: DSC thermograms for the two courses and three samples.

A second endothermic peak appears around +65°C on the first scan. According to the results of Wang et al. [1], this value corresponds to the glass transition temperature of unplasticized PVC. This result is in agreement with the open literature [16, 37] Indeed, it is well-known that the type and percentage of plasticizer lead to a drop in the glass transition temperature. The second scan curve is straight, suggesting complete miscibility between PVC and plasticizers.

A third peak is detected on the first scan around +240°C, as shown in Figure 4. On the second scan, this peak is shifted to above +250°C. These are exothermic peaks. A comparison between the TGA thermogram and the DSC scan leads to the conclusion that this peak corresponds to the beginning of the material degradation, which occurs around +260°C.

3.4. Dynamic mechanical analysis

DMA tests have been performed at 1 Hz for temperatures ranging from -100°C to 120°C. The results are presented in Figure 5 for storage modulus, loss modulus and tan delta ($\tan\delta$) curves. The $\tan\delta$ curve is defined as the ratio between the loss modulus and the storage modulus.

According to the $\tan\delta$ curve, the glass transition region, at 1 Hz, extends from -40°C to 80°C. Close to the beginning of the glass transition region, a peak is observed at around -30°C on the loss modulus curve, whereas another peak is observed on the $\tan\delta$ curve, at around 0°C. In the literature [38-40], a large discrepancy is observed between DMA T_g given by the $\tan\delta$ peak and DSC T_g. However, Achorn and Ferrillo [36] determine a DMA T_g in agreement

with DSC T_g by considering the glass transition temperature as the average of the loss modulus and $\tan\delta$ peak temperature measured at 1 rad/s (around 0.15 Hz). According to this procedure, T_g is measured around -15°C at 1 Hz, higher than DSC T_g due to relative higher frequency (supposedly around 0.15 Hz according to the work of Achorn and Ferrillo [41]).

The discrepancy observed in the glass transition temperature between DSC and DMA can be explained by a) these two techniques involve different material states during the analysis, b) since the operating conditions between DSC and DMA differ, the thermal equilibrium within the material is not the same. Thus, because the glass transition is a thermally activated process, it is expected to observe such discrepancy between two different measures. Moreover, DSC measurements are known to be more thermodynamically stable than DMA where thermal gradients can occur inside the sample whose geometry and weight are quite different from DSC.

Throughout the entire glass transition region, we observe a major drop in the storage modulus, from 3 GPa to around 2 MPa. Thus, for temperatures below -50°C, PPVC is in its glassy state, while for temperatures above 80°C, this material is in its rubbery state.

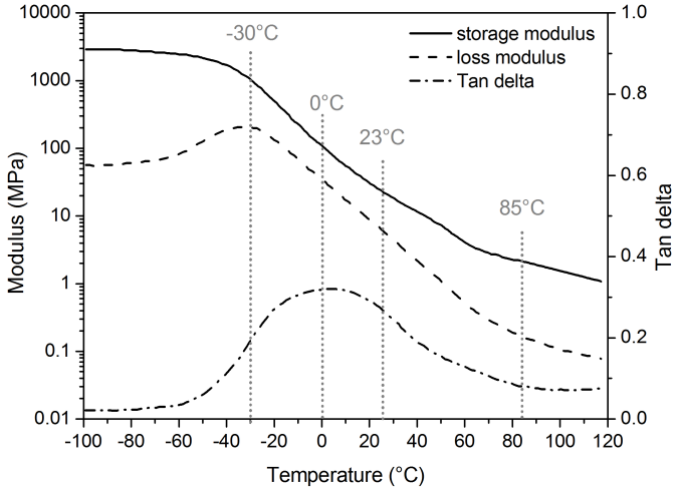

Figure 5: DMA curve plotted at 1 Hz.

3.5. Thermomechanical characterization

The thermomechanical behavior of PPVC has been investigated at low and high strain rates, for temperatures ranging from -30°C to 85°C. This corresponds to the glass transition region according to Figure 5. During the lifetime of the structure, the temperature of the material can vary between -30°C and 85°C. Thus, this temperature range is classically used by the automotive industry to validate their materials. Tensile tests have been performed at low

strain rates, until the failure of the material or the maximum displacement of the machine is achieved. Dynamic tests have been performed at high strain rates. The level of strain reached at the end of the dynamic test is not relevant. Thus, the level of strain reached under dynamic loading will not be analyzed, as we cannot link it to the failure. Equilibrium was reached for each test presented in this study.

3.5.1. Mechanical behavior of PPVC

Representative true stress-strain curves are plotted in Figure 6. The temperature sensitivity of PPVC at 0.03 s^{-1} is plotted in Figure 6a and its strain rate sensitivity is plotted in Figure 6b, Figure 6c and Figure 6d for three temperatures (-30°C, 23°C and 85°C). For low strain rates, specimens have been tested under tensile loading, whereas for high strain rates, specimens were tested under compressive loading. However, no barreling effect is observed in dynamic conditions due to the low thickness/diameter ratio. Evolution of the thermomechanical behavior of PPVC is observed: from a viscoelastic-viscoplastic behavior to a rubbery behavior.

The true stress-strain curves presented in Figure 6 show two stages: a short stage at the beginning of the curve corresponding to elastic, viscoelastic behavior and a second stage characterized by non-linearity of the stress-strain curves. The slope of the curves in the second phase decreases as temperature increases. The material properties, elastic modulus and yield stress, increase when the temperature decreases as shown in Figure 6a. For all specimens, no necking was observed during tensile tests. For the different tested strain rates and temperatures, all stress-strain curves show a major strain hardening. All specimens have been broken in the gauge length except those tested at 85°C, where no failure was observed, as shown in Figure 6a.

The strain rate sensitivity of PPVC is presented in Figure 6b, Figure 6c and Figure 6d for three temperatures: firstly, -30°C, close to the glass transition region (see Figure 6b); secondly, at room temperature in the rubbery state (see Figure 6c); thirdly, at 85°C (see Figure 6d). For all temperatures, the elastic modulus and the yield stress increase when the strain rate increases.

At low temperatures exemplified by Figure 6b, a change of mechanical behavior is observed between dynamic and quasi-static loadings. At high strain rate, PPVC exhibits a glassy

behavior, whereas at low strain rate, it exhibits a viscoelastic-viscoplastic behavior. Then, the material is in its glass transition region ($T_g = -32$°C, see DSC curves in Figure 4). At high strain rates, PPVC demonstrates a classical mechanical behavior under compression loading; after a linear elastic response, a non-linear response appears before the yield point. After this point, the material exhibits a plastic behavior. The viscoplasticity of the material can be divided into two domains: an initial strain softening domain, followed by a strain hardening domain due to polymer chain alignment. At low strain rates, there is no strain softening. The viscoelastic stage is directly followed by the strain hardening domain, until specimen failure occurs.

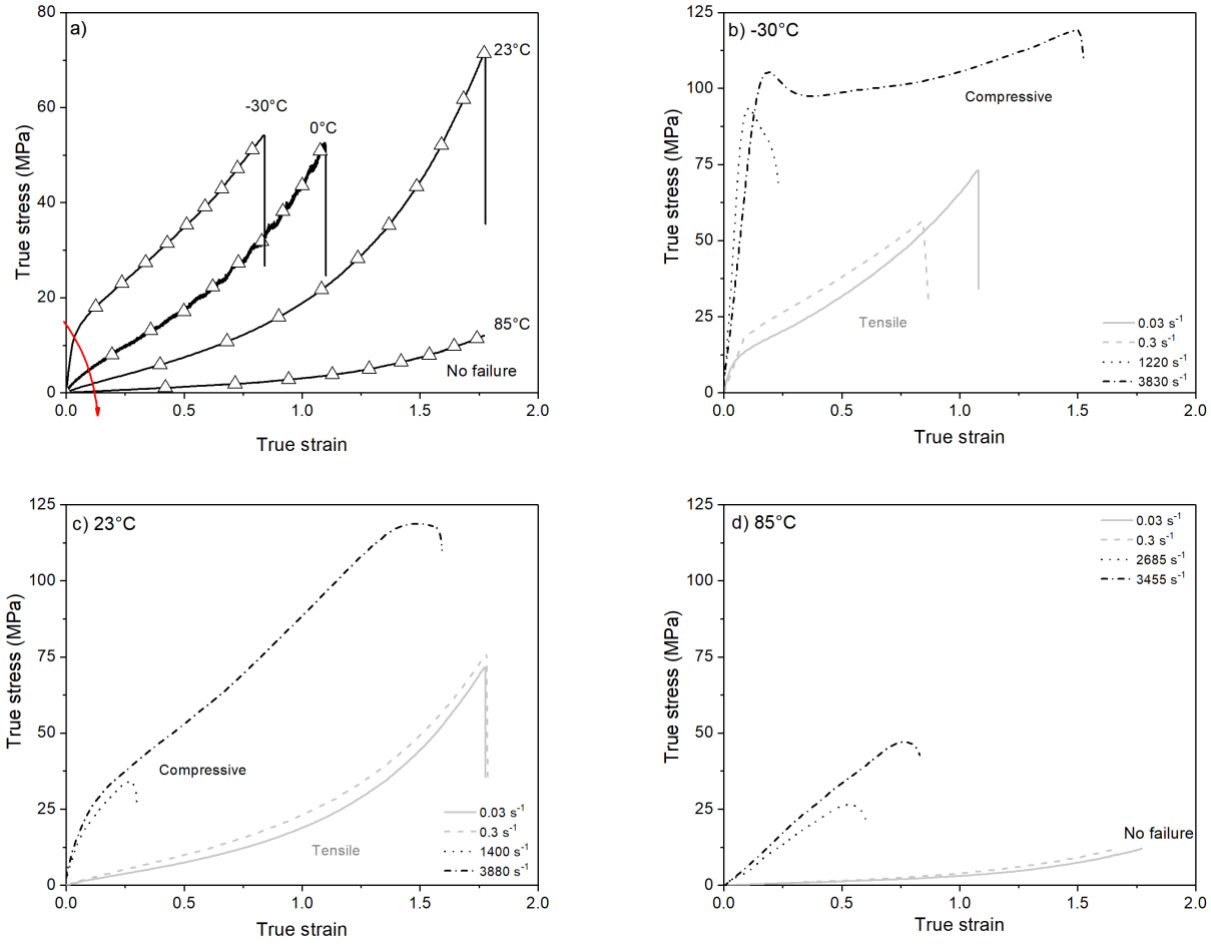

Figure 6: Experimental true stress-true strain curves under uniaxial quasi-static tensile loading and dynamic compressive loadings. a) Temperature sensitivity at 0.03s^{-1}. Strain rate sensitivity at b) -30°C, c) 23°C and d) 85°C.

At room temperature, a change of behavior is also observed between high and low strain rates (see Figure 6c). The mechanical behavior at high strain rates is close to that observed at low strain rates and temperature (see Figure 6a). Thus, at room temperature and a high strain rate, PPVC exhibits a viscoelastic-viscoplastic behavior. At room temperature and low strain

rate (see Figure 6c) and at 85°C at all strain rates (see Figure 6d), PPVC presents a rubbery behavior.

By comparing Figure 6b, Figure 6c and Figure 6d, the temperature sensitivity of PPVC at high strain rate is clearly identified on the evolution of the flow stress. Moreover, the behavior of PPVC gradually changes from an elastic-viscoplastic behavior to a viscoelastic-viscoplastic one, followed by a hyper-viscoelastic behavior [42, 43].

3.5.2. Temperature and strain rate sensitivity of material properties

Elastic modulus, yield strain, yield stress, strain at break-point and stress at break-point have been analyzed using the true stress-strain curves presented above. At low strain rates due to the low stiffness of the material, we use the nominal stress-strain curves to determine an accurate value for the elastic modulus and the onset of yield. Young's modulus is calculated from the initial slope of the true (or nominal) stress-strain curves. When the elastic-viscoelastic behavior of PPVC is followed by strain softening, the yield stress is taken as the maximum between these two stages. In cases where the stress-strain curves do not show a local maximum, the yield stress is defined as the intersection of the elastic and the plastic slopes.

Temperature sensitivity of material properties at low strain rates

For a better understanding of the temperature sensitivity on the mechanical properties of PPVC, these are plotted in Figure 7. The elastic modulus (see Figure 7a), the yield stress, the stress at break-point (see Figure 7b), the yield strain and the elongation at break-point (see Figure 7c) were plotted. Two strain rates are investigated. Figure 7a shows a non-linear relationship between elastic modulus and temperature. At -30°C, a discrepancy is found for the elastic modulus, due to the proximity of this temperature to the glass transition temperature. Above this temperature, the material is in a rubbery state. A non-linear evolution was observed. At low temperature, and for a strain rate of 0.3 s^{-1}, the elastic modulus could not be measured due to limitations of the experimental setup. In the rubbery region, between 23°C and 85°C, the experimental data for the two strain rates are superimposed. This means that the strain rate sensitivity of PPVC is not significant in the rubbery region.

The temperature sensitivity of the yield stress and the stress at break-point is plotted in Figure 7b. The yield stress decreases non-linearly as the temperature increases and it increases with the strain rate. The stress at break-point increases when the temperature increases or when the strain rate decreases. At 85°C, the samples did not break and the maximum displacement of the testing machine is reached before material failure. The strain rate sensitivity of PPVC is considerable at low temperature.

In Figure 7c, the temperature sensitivity of the yield strain and the elongation at break-point are plotted for two strain rates: 0.03 s^{-1} and 0.3 s^{-1}. These properties increase with temperature. The yield strain exhibits a non-linear dependence on temperature, where a change of slope is observed at 0°C. Moreover, the yield strain increases when the strain rate increases. Contrary to the yield strain, the elongation at break-point does not seem to be influenced by the glass transition temperature. As for the stress at break-point, the elongation is linearly dependent on the inverse of the temperature.

The miscibility of plasticizers with PVC results in the formation of a physical network between the two materials. The plasticizer in this network [44] causes chain slippage and consequently high elongation at break-point for plasticizer components in blends [7].

All results presented in these sections comes from a set of data. Thus, all include standard deviation. However, it can appear, for some results, very small standard deviation which are not visible on the figures.

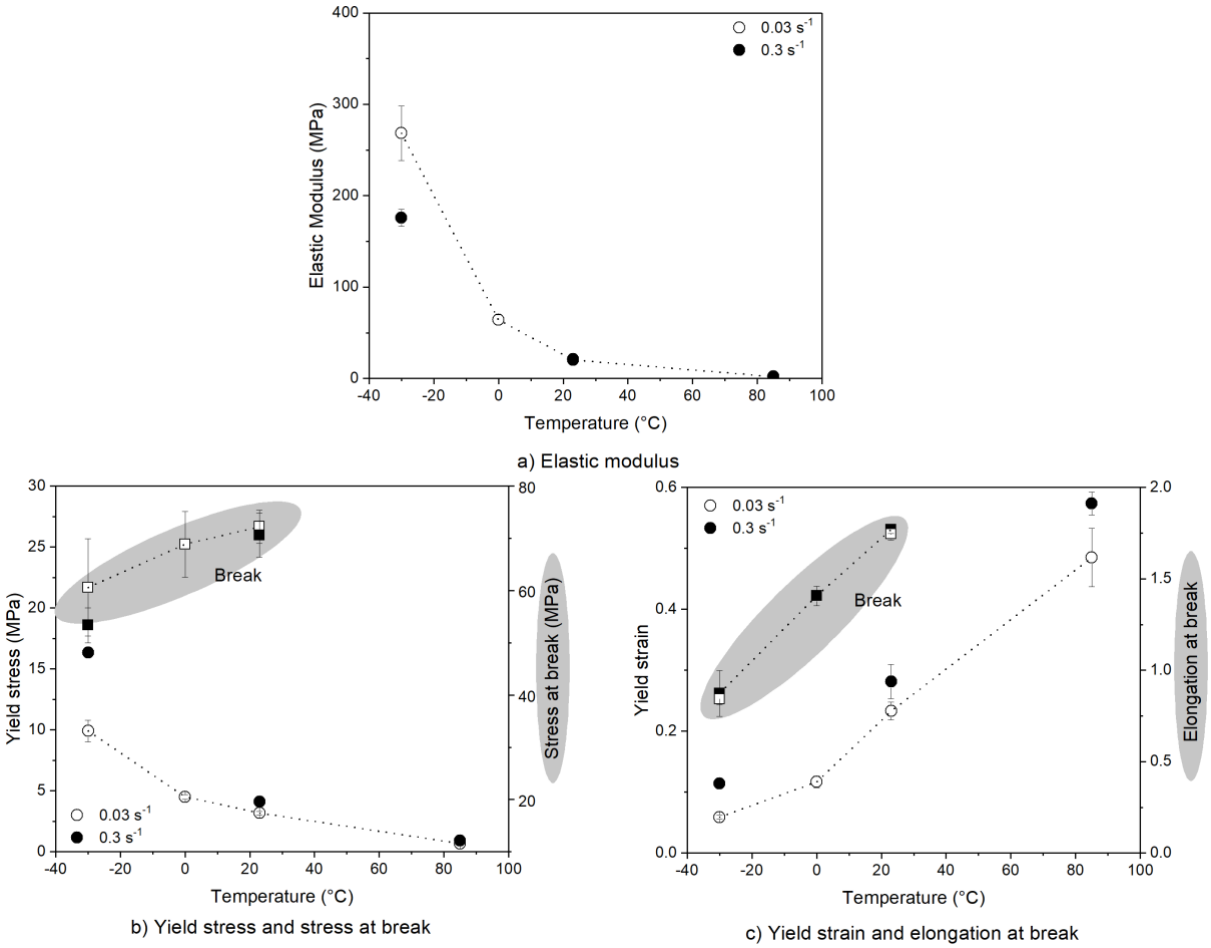

Figure 7: Temperature sensitivity at $\dot{\varepsilon} = 0.03\ s^{-1}$ and at $\dot{\varepsilon} = 0.3\ s^{-1}$ a) elastic modulus, b) yield stress and stress at break and c) yield strain and elongation at break.

Strain rate sensitivity of material properties

The strain rate dependence of the elastic modulus, yield stress and yield strain at three temperatures (-30°C, 23°C, 85°C) are presented in Figure 8a, Figure 8b and Figure 8c, respectively. -30°C is close to the glass transition temperature, while 23°C and 85°C are in the rubbery region. At high strain rates and 85°C, these material properties are not reported due to the hyper-elastic behavior of the material for these coupled conditions.

In Figure 8a, we observe a major discrepancy of the elastic modulus at high strain rates. This phenomenon is due to the strong strain rate sensitivity of the elastic modulus in the glass transition region and a non-optimal dynamic equilibrium. Between quasi-static and dynamic loadings, an increase of the elastic modulus is observed.

Figure 8b shows an increase of yield stress when the temperature decreases and the strain rate increases. At 23°C, the yield stress is bi-linearly dependent on the log of the strain rate. A

drop in yield stress is observed between -30°C and 23°C due to the passage of the glass transition region.

In Figure 8c, the strain rate dependency of the yield strain is plotted for the three temperatures tested. At low strain rates, the yield strain increases when the temperature and strain rate increase. However, at high strain rates, for the two temperatures considered (-30°C and 23°C), the yield strain increases when the strain rate increases but decreases when the temperature increases. Two assumptions can be formulated to explain this change of yield strain mechanical behavior between low and high strain rates. Firstly, we can consider that the modification in behavior is due to the change of behavior between quasi-static and dynamic loading upon the glass transition to a glassy region at -30°C and from rubbery to a glass transition region at 23°C. Secondly, the change of behavior could be due to an increase of viscoelasticity at 23°C, as observed in Figure 6. The same level of yield strain is obtained for the couples (low strain rates, 30°C) and (high strain rates, 23°C), as shown in Figure 8c. At 85°C, in the rubbery region, a major discrepancy is observed due to the hyper-elastic behavior of the material at this temperature.

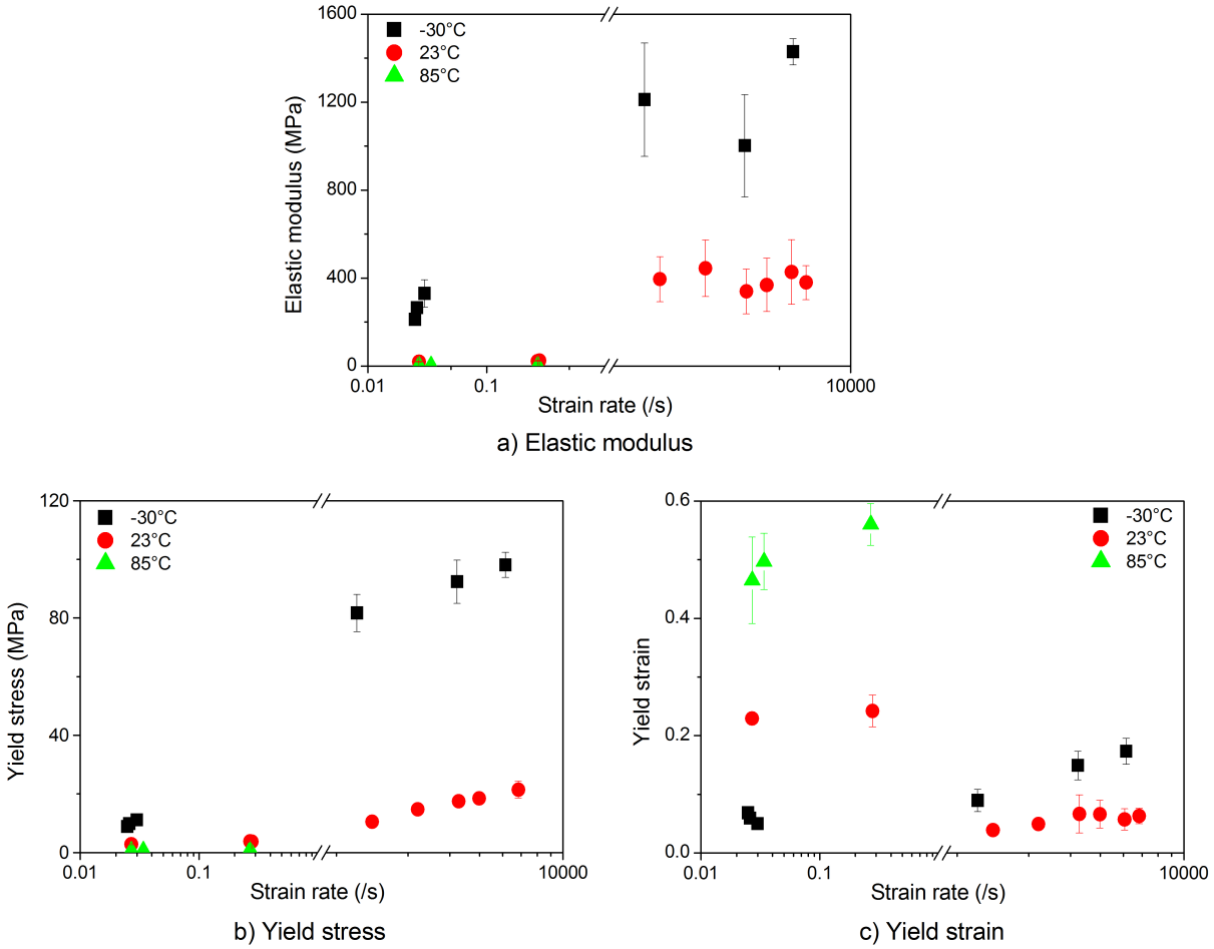

Figure 8: Strain rate sensitivity at three temperatures (-30°C, 23°C, 85°C) a) elastic modulus, b) yield stress and c) yield strain.

4. Modelling

4.1. Storage modulus

Several models described in the literature allow the evolution of the storage modulus from the glassy region to the rubbery region to be modelled [45-48]. Among them, the model developed by Mahieux and Reifsnider [45, 46] and improved by Richeton et al. [47] has been validated for a large number of polymers (amorphous and semi-crystalline). The model is based on Weibull statistics to simulate the breakage of the secondary links:

$$E(T) = (E_1 - E_2)\exp\left(-\left(\frac{T}{T_\beta}\right)^{m_1}\right) + (E_2 - E_3)\exp\left(-\left(\frac{T}{T_g}\right)^{m_2}\right) + E_3\exp\left(-\left(\frac{T}{T_m}\right)^{m_3}\right) \quad (6)$$

where E_1, E_2 and E_3 are the instantaneous moduli of the material at the beginning of each region (glassy, glass transition and rubbery). T_β, T_g and T_m are the temperatures of each

transition (secondary relaxation, glass transition and melting temperature) and m_i are the Weibull moduli associated with the breakage of the secondary links.

This model is used to simulate the temperature sensitivity of the storage modulus observed at 1 Hz for the DMA test (see Figure 5). The comparison between the DMA experimental results and the numerical predictions are presented in Figure 9 for linear and logarithmic scales. A good agreement is observed between the experimental results and the numerical model calibrated with the parameters described in Table 1.

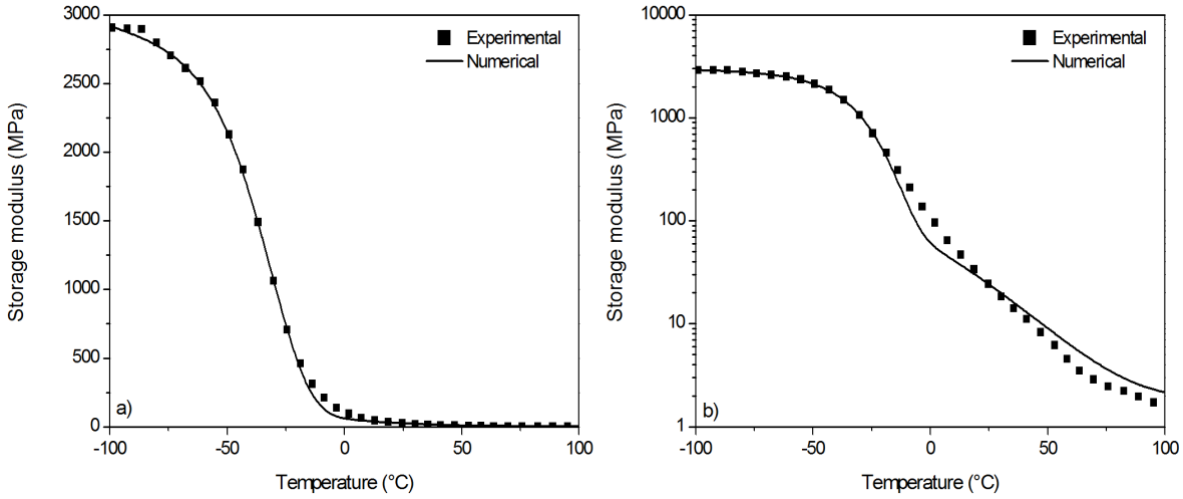

Figure 9: Numerical modelling of the storage modulus. Comparison between experimental results and numerical prediction in a) linear and b) logarithmic scale.

Table 1: Model parameters for the storage modulus (eq. (1)

E_1(MPa)	E_2 (MPa)	E_3 (MPa)	T_β(K)	T_g (K)	T_m (K)	m_1	m_2	m_3
3204	2413	1.8	210	243	700	3.5	15.9	25

4.2. Yield stress

During recent decades, numerous models [47, 49-53] have been developed to model the strain rate and temperature dependencies of the yield stress. These models consider the yield stress as a thermally activated process. They allow modelling of the yield strength of glassy polymers over a wide range of strain rates and temperatures. However, few models allow reproduction of the yield stress in the glass transition and rubbery regions. Among those that do so, the cooperative model developed in our team by Richeton et al. [47, 54] takes into account the drop of yield strength due to the glass transition temperature.

The cooperative model considers the cooperative jump motions of n polymer chain segments. Lower than T_g, it takes on the existence of an internal stress σ_i, structural parameter which depicts the thermal history of the material. Higher than T_g, the internal stress is null, allowing the flow of polymer chain segments. Thus, as a function of temperature, the internal stress is defined as [41]:

$$\sigma_i(T) = \begin{cases} \sigma_i(0) - mT & if\ T < T_g \\ 0 & if\ T \geq T_g \end{cases} \tag{7}$$

with $\sigma_i(0)$ the internal stress at 0K and m a material parameter close to $\sigma\_i(0)/T_g$. According to Fotheringham and Cherry [55, 56], the yield stress σ_y is given by:

$$\sigma_y = \sigma_i(T) + \frac{2kT}{V}\sinh^{-1}\left(\frac{\dot{\varepsilon}}{\dot{\varepsilon}^*(T)}\right)^{1/n} \tag{8}$$

with k the Bolzmann constant, T the absolute temperature, $\dot{\varepsilon}$ the strain rate, V the activation volume, $\dot{\varepsilon}^*$ the characteristic strain rate and n describing the cooperative character of the yield process. The temperature sensitivity of the characteristic strain rate is defined by:

$$\dot{\varepsilon}^* = \begin{cases} \dot{\varepsilon}_0 \exp\left(-\frac{\Delta H_\beta}{RT}\right) & if\ T < T_g \\ \dot{\varepsilon}_0 \exp\left(-\frac{\Delta H_\beta}{RT_g}\right)\exp\left(\frac{\ln 10\ c_1\left(T - T_g\right)}{c_2 + T - T_g}\right) & if\ T \geq T_g \end{cases} \tag{9}$$

with ΔH_β the β activation energy, c_1, c_2 the WLF parameters, R the gas constant and $\dot{\varepsilon}_0$ a pre-exponential constant.

To build the master curve for the yield stress, a referenced temperature T_{ref} is chosen and the time/temperature superposition principle is applied. The horizontal and vertical shifts are given by:

$$\begin{cases} \Delta(\log\dot{\varepsilon}) = \log\dot{\varepsilon}\left(T_{ref}\right) - \log(\dot{\varepsilon}) \\ \Delta\left(\frac{\sigma_y}{T}\right) = \frac{\sigma_y(T_{ref})}{T_{ref}} - \frac{\sigma_y(T)}{T} \end{cases} . \tag{10}$$

In Figure 10, the master curve is built at -30°C using the parameter presented in Table 2. An important dispersion of the experimental results is observed at high strain rates. However, a good agreement between experimental results and the numerical prediction can still be observed from quasi-static to dynamic strain rates.

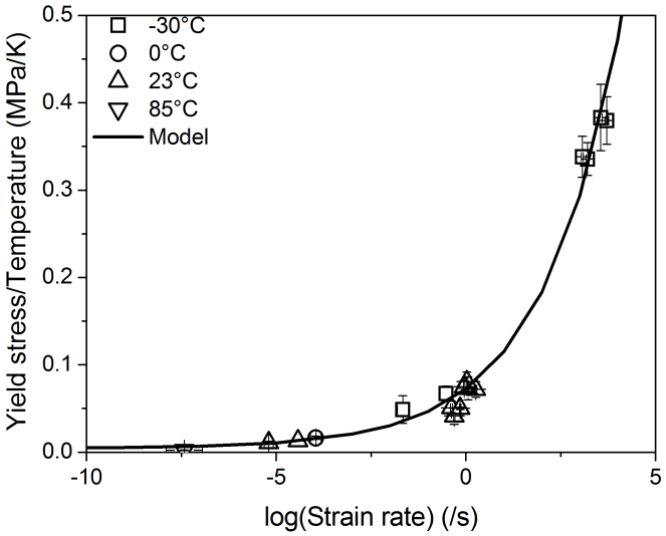

Figure 10: Master curve built at -30°C for the PPVC tested in uniaxial tension for low strain rates and uniaxial compression for high strain rates.

Table 2: Model parameters for the cooperative model used to build the master curve at -30°C.

ΔH_β (kJ/mol)	$\sigma_i(0)$ (MPa)	m (MPa.K^{-1})	V (m^3)	$\dot{\varepsilon}_0$ (s^{-1})	n
10	5	0.016	3.6E-29	1.5E7	4.78

5. Conclusion

Thermal, mechanical and microscopic investigations have been performed on a multilayered PPVC for the automotive industry. Degassing phenomena occurring during the manufacturing process of the PPVC sheets induces 4% of voiding and increase to 6.7% after tensile tests. Moreover, testing specimens reveal the presence of sodium aluminosilicate clusters classically used component to stabilize PVC melts. These particles are parts of the 10% of additives added in the polymer formulation and the only one remaining after the thermal degradation of the material.

DSC measurements and DMA feature the temperature range of the study into the glass transition region of the material. This one is quite wide and extends from -40°C to 80°C. The thermomechanical tests performed in that study clearly illustrate the change of behavior of PPVC over the temperature range. From the glass transition region to the rubbery region for quasi-static tests and from glassy region to rubbery region for dynamic range, all the spectrum of behavior is analyzed. In the investigated range of temperature and strain rate, elastic modulus, yield stress and yield strain exhibit a non-linear behavior with a change of slope

around 0°C (peak of the tan δ curve). In the case of the stress at break and elongation at break-point, linear evolution is observed in the studied temperature range. Modelling of the storage modulus and yield stress were also performed and a good agreement was found between the numerical prediction and the experimental results.

Acknowledgements

The authors thank Professor Christophe Fond and Assistant Professor Rigoberto Ibarra for their helpful discussions.

References

[1] Y. Wang, E.M. Arruda, P.A. Przybylo, Characterization and Constitutive Modeling of a Plasticized Poly(vinyl Chloride) for a Broad Range of Strain Rates, Rubber Chemistry and Technology. 74 (2001) 560–573. doi:10.5254/1.3544957.

[2] M. Aubin, R.E. Prud'homme, Analysis of the glass transition temperature of miscible polymer blends, Macromolecules. 21 (1988) 2945–2949. doi:10.1021/ma00188a010.

[3] X. Lu, R.A. Weiss, Relationship between the glass transition temperature and the interaction parameter of miscible binary polymer blends, Macromolecules. 25 (1992) 3242–3246. doi:10.1021/ma00038a033.

[4] G. Pezzin, F. Zilio-Grandi, P. Sanmartin, The dependence of the glass transition temperature on molecular weight for polyvinylchloride, European Polymer Journal. 6 (1970) 1053–1061. doi:10.1016/0014-3057(70)90038-8.

[5] J.H. Gibbs, E.A. DiMarzio, Nature of the Glass Transition and the Glassy State Nature of the Glass Transition and the Glassy State, AIP The Journal of Chemical Physics. 28 (1958) 373–383.

[6] T. Somcynsky, D. Patterson, The glass transition and the reduced temperature of polymeric liquids, J. Polym. Sci. 62 (1962) S151–S155. doi:10.1002/pol.1962.1206217460.

[7] K.T. Varughese, G.B. Nando, S.K. De, S.K. Sanyal, Tensile and tear failure of plasticized poly (vinyl chloride)/epoxidized natural rubber miscible blends, J Mater Sci. 24 (1989) 3491–3496. doi:10.1007/BF02385730.

[8] C.-S. Ha, Y. Kim, W.-K. Lee, W.-J. Cho, Y. Kim, Fracture toughness and properties of plasticized PVC and thermoplastic polyurethane blends, Polymer. 39 (1998) 4765–4772. doi:10.1016/S0032-3861(97)10326-3.

[9] K. J. Roy, T. V. Anjali, A. Sujith, Asymmetric membranes based on poly(vinyl chloride): effect of molecular weight of additive and solvent power on the morphology and performance J Mater Sci (2017) 52: 5708. https://doi.org/10.1007/s10853-017-0807-1

[10] M.J. Kendall, C.R. Siviour, Strain rate dependence in plasticized and un-plasticized PVC, EPJ Web of Conferences. 26 (2012). doi:10.1051/epjconf/20122602009.

[11] M.J. Kendall, C.R. Siviour, Rate dependence of poly(vinyl chloride), the effects of plasticizer and time–temperature superposition, Proceedings of the Royal Society of London A: Mathematical, Physical and Engineering Sciences. 470 (2014). doi:10.1098/rspa.2014.0012.

[12] Zhang, H., Hu, X., Chen, Y. et al. Dynamic rheological property and membrane formation of mechanochemically modified polyvinylchloride, J Mater Sci (2015) 50: 4371. https://doi.org/10.1007/s10853-015-8991-3

[13] A. Mulliken D., S. Soong Y., M. Boyce C., R. Cohen E., High-rate thermomechanical behavior of poly(vinyl chloride) and plasticized poly(vinyl chloride), J. Phys. IV France. 134 (2006) 217–223. doi:10.1051/jp4:2006134033.

[14] L.M. Matuana, C.B. Park, J.J. Balatinecz, The effect of low levels of plasticizer on the rheological and mechanical properties of polyvinyl chloride/newsprint-fiber composites, J Vinyl Addit Technol. 3 (1997) 265–273. doi:10.1002/vnl.10204.

[15] A. Marcilla, M. Beltrán, Effect of the plasticizer concentration and heating rate on the thermal decomposition behaviour of PVC plastisols. Kinetic analysis, Polymer Degradation and Stability. 60 (1998) 1–10. doi:10.1016/S0141-3910(96)00124-3.

[16] M. Altenhofen da Silva, M.G. Adeodato Vieira, A.C. Gomes Maçumoto, M.M. Beppu, Polyvinylchloride (PVC) and natural rubber films plasticized with a natural polymeric plasticizer obtained through polyesterification of rice fatty acid, Polymer Testing. 30 (2011) 478–484. doi:10.1016/j.polymertesting.2011.03.008.

[17] G. Ceccorulli, M. Pizzoli, M. Scandola, Composition dependence of the glass transition temperature of polymer-diluent systems: 1. Experimental evidence of a dual behaviour in plasticized PVC, Polymer. 28 (1987) 2077–2080. doi:10.1016/0032-3861(87)90044-9.

[18] T. Rehm, The compression set of plasticized PVC, J Vinyl Addit Technol. 3 (1997) 286–291. doi:10.1002/vnl.10208.

[19] V.J.R.R. Pita, E.E.M. Sampaio, E.E.C. Monteiro, Mechanical properties evaluation of PVC/plasticizers and PVC/thermoplastic polyurethane blends from extrusion processing, Polymer Testing. 21 (2002) 545–550. doi:10.1016/S0142-9418(01)00122-2.

[20] A. Elicegui, J.J. del Val, V. Bellenger, J. Verdu, A study of plasticization effects in poly(vinyl chloride), Polymer. 38 (1997) 1647–1657. doi:10.1016/S0032-3861(96)00671-4.

[21] S. Thomas, B. Kuriakose, B.R. Gupta, S.K. De, Scanning electron microscopy studies on tensile, tear and abrasion failure of plasticized poly (vinyl chloride) and copolyester thermoplastic elastomers, J Mater Sci. 21 (1986) 711–716. doi:10.1007/BF01145545.

[22] C.A. Bernard, N. Bahlouli, C. Wagner-Kocher, S. Ahzi and Y. Rémond Impact behaviour of an innovative plasticized poly(vinyl chloride) for the automotive industry https://doi.org/10.1051/epjconf/20159402013

[23] Julie Diani, Pierre Gilormini, Carole Frédy , Ingrid Rousseau, Predicting thermal shape memory of crosslinked polymer networks from linear viscoelasticity, International Journal of Solids and Structures, Volume 49, Issue 5, 1 March 2012, Pages 793-799

[24] M. Dixit, V. Mathur, S. Gupta, M. Baboo, K. Sharma, N. S. Saxena, Investigation of miscibility and mechanical properties of PMMA/PVC blends, Optoelectronics And Advanced Materials – Rapid Communications Vol. 3, No. 10, October 2009, p. 1099 - 1105

[25] R. Matadi, E. Hablot, K. Wang, N. Bahlouli, S. Ahzi, L. Avérous, High strain rate behaviour of renewable biocomposites based on dimer fatty acid polyamides and cellulose fibres, Composites Science and Technology. 71 (2011) 674–682. doi:10.1016/j.compscitech.2011.01.010.

[26] D. Pessey, N. Bahlouli, S. Pattofatto, S. Ahzi, Polymer composites for the automotive industry: characterisation of the recycling effect on the strain rate sensitivity, International Journal of Crashworthiness. 13 (2008) 411–424. doi:10.1080/13588260802030745.

[27] K. Wang, F. Addiego, A. Laachachi, B. Kaouache, N. Bahlouli, V. Toniazzo, D. Ruch, Dynamic behavior and flame retardancy of HDPE/hemp short fiber composites: Effect of coupling agent and fiber loading, Composite Structures. 113 (2014) 74–82. doi:10.1016/j.compstruct.2014.03.009.

[28] N. Bahlouli, D. Pessey, C. Raveyre, J. Guillet, S. Ahzi, A. Dahoun, J.M. Hiver, Recycling effects on the rheological and thermomechanical properties of polypropylene-based composites, Materials & Design. 33 (2012) 451–458. doi:10.1016/j.matdes.2011.04.049.

[29] O.. Lee, M.. Kim, Dynamic material property characterization by using split Hopkinson pressure bar (SHPB) technique, Nuclear Engineering and Design. 226 (2003) 119–125. doi:10.1016/S0029-5493(03)00189-4.
[30] K. Wang, F. Addiego, N. Bahlouli, S. Ahzi, Y. Rémond, V. Toniazzo, Impact response of recycled polypropylene-based composites under a wide range of temperature: Effect of filler content and recycling, Composites Science and Technology. 95 (2014) 89–99. doi:10.1016/j.compscitech.2014.02.014.
[31] K. Worschech, P. Wedl, E. Fleischer, F. Loeffelholz, M. Jaeckel, Stabilizer for chlorine-containing olefin polymers, a process for its production and polymers containing the stabilizer, (1991).
[32] F. Gong, M. Feng, C. Zhao, S. Zhang, M. Yang, Thermal properties of poly(vinyl chloride)/montmorillonite nanocomposites, Polymer Degradation and Stability. 84 (2004) 289–294. doi:10.1016/j.polymdegradstab.2003.11.003.
[33] Q. Yao, C.A. Wilkie, Thermal degradation of PVC in the presence of polystyrene, J Vinyl Addit Technol. 7 (2001) 26–36. doi:10.1002/vnl.10261.
[34] Y. Soudais, L. Moga, J. Blazek, F. Lemort, Coupled DTA–TGA–FT-IR investigation of pyrolytic decomposition of EVA, PVC and cellulose, Journal of Analytical and Applied Pyrolysis. 78 (2007) 46–57. doi:10.1016/j.jaap.2006.04.005.
[35] R. Bacaloglu, M. Fisch, Degradation and stabilization of poly(vinyl chloride). I. Kinetics of the thermal degradation of poly(vinyl chloride), Polymer Degradation and Stability. 45 (1994) 301–313.
[36] A. Marongiu, T. Faravelli, G. Bozzano, M. Dente, E. Ranzi, Thermal degradation of poly(vinyl chloride), Journal of Analytical and Applied Pyrolysis. 70 (2003) 519–553. doi:10.1016/S0165-2370(03)00024-X.
[37] A. Lindström, M. Hakkarainen, Environmentally friendly plasticizers for poly(vinyl chloride)—Improved mechanical properties and compatibility by using branched poly(butylene adipate) as a polymeric plasticizer, J. Appl. Polym. Sci. 100 (2006) 2180–2188. doi:10.1002/app.23633.
[38] J.M. Barton, Thermoanalytical study of an epoxy resin crosslinked with an aliphatic polyamine, Thermochimica Acta. 30 (1979) 153–161. doi:10.1016/0040-6031(79)85050-9.
[39] P.L. Kumler, G.A. Machajewski, J.J. Fitzgerald, L.R. Denny, S.E. Keinath, R.F. Boyer, Detection of Tll in styrene-ethyl acrylate random copolymers by differential scanning calorimetry and dynamic mechanical analysis, Macromolecules. 20 (1987) 1060–1065. doi:10.1021/ma00171a032.
[40] B. Cassel, B. Twombly, Glass transition determination by thermomechanical analysis, a dynamic mechanical analyzer, and a differential scanning calorimeter, in: Materials Characterization by Thermomechanical Analysis, ASTM International, 1991.
[41] P.J. Achorn, R.G. Ferrillo, Comparison of thermal techniques for glass transition measurements of polystyrene and cross-linked acrylic polyurethane films, Journal of Applied Polymer Science. 54 (1994) 2033–2043.
[42] V. Oshmyan, S. Patlazhan, Y. Remond, Simulation of small-strain deformations of semi-crystalline polymer: Coupling of structural transformations with stress-strain response, Journal of Materials Science. 39 (2004) 3577–3586. doi:10.1023/B:JMSC.0000030709.19754.28.
[43] S. Patlazhan, Y. Remond, Structural mechanics of semicrystalline polymers prior to the yield point: a review, J Mater Sci. 47 (2012) 6749–6767. doi:10.1007/s10853-012-6620-y.
[44] V.J.R.R.PitaaE.E.M.SampaiobE.E.C.Monteiroa, Mechanical properties evaluation of PVC/plasticizers and PVC/thermoplastic polyurethane blends from extrusion processing, https://doi.org/10.1016/S0142-9418(01)00122-2
[45] C.. Mahieux, K.. Reifsnider, Property modeling across transition temperatures in polymers: a robust stiffness–temperature model, Polymer. 42 (2001) 3281–3291. doi:10.1016/S0032-3861(00)00614-5.

[46] C.A. Mahieux, K.L. Reifsnider, Property modeling across transition temperatures in polymers: application to thermoplastic systems, Journal of Materials Science. 37 (2002) 911–920. doi:10.1023/A:1014383427444.
[47] J. Richeton, S. Ahzi, L. Daridon, Y. Rémond, A formulation of the cooperative model for the yield stress of amorphous polymers for a wide range of strain rates and temperatures, Polymer. 46 (2005) 6035–6043. doi:10.1016/j.polymer.2005.05.079.
[48] R.B. Dupaix, M.C. Boyce, Constitutive modeling of the finite strain behavior of amorphous polymers in and above the glass transition, Mechanics of Materials. 39 (2007) 39–52. doi:10.1016/j.mechmat.2006.02.006.
[49] H. Eyring, Viscosity, Plasticity, and Diffusion as Examples of Absolute Reaction Rates, The Journal of Chemical Physics. 4 (1936) 283–291.
[50] R.E. Robertson, Theory for the Plasticity of Glassy Polymers, The Journal of Chemical Physics. 44 (1966) 3950–3956.
[51] A.S. Argon, A theory for the low-temperature plastic deformation of glassy polymers, Philosophical Magazine. 28 (1973) 839–865. doi:10.1080/14786437308220987.
[52][P.B. Bowden, S. Raha, A molecular model for yield and flow in amorphous glassy polymers making use of a dislocation analogue, Philosophical Magazine. 29 (1974) 149–166. doi:10.1080/14786437408213560.
[53] T. Ree, H. Eyring, Theory of Non-Newtonian Flow. I. Solid Plastic System, Journal of Applied Physics. 26 (1955) 793–800.
[54] J. Richeton, S. Ahzi, K.S. Vecchio, F.C. Jiang, R.R. Adharapurapu, Influence of temperature and strain rate on the mechanical behavior of three amorphous polymers: Characterization and modeling of the compressive yield stress, International Journal of Solids and Structures. 43 (2006) 2318–2335. doi:10.1016/j.ijsolstr.2005.06.040.
[55] D. Fotheringham, B.W. Cherry, C. Bauwens-Crowet, Comment on “the compression yield behaviour of polymethyl methacrylate over a wide range of temperatures and strain-rates,” J Mater Sci. 11 (1976) 1368–1371. doi:10.1007/BF00545162.
[56] D.G. Fotheringham, B.W. Cherry, The role of recovery forces in the deformation of linear polyethylene, J Mater Sci. 13 (1978) 951–964. doi:10.1007/BF00544690.